NASA CONTRACTOR REPORT

NASA CR-795

NASA CR-795

THE EFFECT OF EDGE CONSTRAINT ON THE BUCKLING OF SANDWICH AND RING-STIFFENED 120 DEGREE CONICAL SHELLS SUBJECTED TO EXTERNAL PRESSURE

by Gerald A. Cohen

Prepared by
AERONUTRONIC, DIVISION OF PHILCO-FORD CORPORATION
Newport Beach, Calif.
for Langley Research Center

NATIONAL AERONAUTICS AND SPACE ADMINISTRATION • WASHINGTON, D. C. • MAY 1967

NASA CR-190

THE EFFECT OF EDGE CONSTRAINT ON THE BUCKLING OF SANDWICH AND RING-STIFFENED 120 DEGREE CONICAL SHELLS SUBJECTED TO EXTERNAL PRESSURE

By Gerald A. Cohen

Prepared under Contract No. NAS 1-5554 by
AERONUTRONIC, DIVISION OF PHILCO-FORD CORPORATION
Newport Beach, Calif.

for Langley Research Center

NATIONAL AERONAUTICS AND SPACE ADMINISTRATION

ABSTRACT

The buckling strength of a 120° truncated conical shell, with dimensions typical of a planetary entry body, subjected to a uniform external pressure reacted at the small edge was studied using Novozhilov shell and ring theory. Five cases of ring-stiffeners at the large end (with a prescribed ring at the small edge) and simply supported edges were treated for each of the following two wall constructions,(1) an aluminum sandwich and (2) a magnesium monocoque with many equally spaced interior rings. For each wall construction the minimum base ring size (of a one-parameter family of rings) required to effectively produce complete edge constraint is determined.

THE EFFECT OF EDGE CONSTRAINT ON THE BUCKLING OF SANDWICH AND RING-STIFFENED 120 DEGREE CONICAL SHELLS SUBJECTED TO EXTERNAL PRESSURE

By Gerald A. Cohen
Aeronutronic, Division of Philco-Ford Corporation

SUMMARY

The buckling strength of a 120-degree truncated conical shell, with dimensions typical of a planetary entry body, subjected to a uniform external pressure reacted at the small edge was studied using a Novozhilov shell and ring theory. Five cases of ring-stiffeners at the large edge (with a prescribed ring at the small edge) and simply supported edges were considered for each of the two following wall constructions: (1) aluminum sandwich, and (2) magnesium monocoque with many equally spaced internal rings. For each wall construction the results indicate that for insufficient edge support, the shell buckles at a low value of critical pressure into a highly inextensional mode with two circumferential waves. As the base ring rigidity increases, the buckling displacements remain essentially unchanged, and the increase in critical pressure results primarily from the increase in flexural strain energy of the base ring in its buckled state. For a sufficiently rigid base ring or simply supported edges, the shell is forced to buckle into a mode with significant extension and seven circumferential waves. In this mode, the buckling displacements are small at the edges, and consequently, the critical pressure is relatively insensitive to edge conditions.

Of the two wall constructions studied, the sandwich construction is superior, withstanding up to 50 percent more pressure than the ring-stiffened monocoque when sufficient edge constraint is provided.

INTRODUCTION

Previous analyses of the buckling of conical shells (Ref. 1) have, in general, been limited to cases of idealized edge conditions, such as simply supported or clamped edges. Inextensional buckling modes, which can lead to reduced buckling loads, are kinematically inadmissible for such edge conditions. On the other hand, the edges of entry body shells are usually supported by ring stiffeners, for which inextensional modes are possible. A recent study of axially compressed cylindrical shells with ring-stiffened edges (Ref. 2) shows that inextensional buckling modes do occur for rings of insufficient rigidity, and considerable ring rigidity is necessary to suppress this type of buckling. Energy considerations indicate that this behavior is not peculiar to cylindrical shells but is characteristic of all shell structures.

The practical problem is then to determine, for a particular configuration, the ring size required to suppress the inextensional buckling modes. The results of Ref. 2 suggest that further increases in ring size are ineffectual, since in the mode into which the shell is forced to buckle the ring strain energy is negligible. As in Ref. 2, the most enlightening approach to this problem is through use of the energy method. However, the present results were obtained through use of a digital computer program which solves the eigenvalue problem associated with the governing differential equations (based on the nonlinear generalization for small finite rotations of Novozhilov's shell equations) for general ring-stiffened orthotropic shells of revolution by means of a modal iteration method. The details of this method are presented in Ref. 3. Linearized prebuckled equilibrium states, which are required as inputs to this program, were obtained through use of a second digital computer program based on the forward integration method of Novozhilov's shell equations presented in Ref. 4.

NOMENCLATURE

A, B	dimensionless parameters of inextensional deformation
d	interior ring spacing
E	Young's modulus
E_1, E_2	meridional and circumferential elastic moduli of equivalent orthotropic material
e_1	meridional extensional strain
I	I_x or I_z for Cases 1, 2, and 3
I_x, I_z, I_{xz}	centroidal moments and product of inertia of ring cross section
J	torsional inertia of ring cross section
M	meridional stress couple of shell wall
n	circumferential wave number of buckling mode

P	axial force per unit of circumferential distance
p	external pressure
r	reference radius of shell cross section
S	area of ring cross section
s	distance along meridian (see Fig. 1)
T_1, T_2	meridional and circumferential stress resultants of shell wall
t	shell wall layer thickness
$\bar{t}$	shell wall thickness effective in resisting stretching
u, v, w	meridional, circumferential and normal displacement amplitudes of shell wall
w_{MAX}	maximum normal displacement
Z	eccentricity of ring centroidal axis measured from inside shell surface, positive for internal rings
α	conical semivertex angle
ΔP	change in P during buckling
η	radial displacement of shell wall
μ	Poisson's ratio
χ	meridional rotation of shell wall

Subscripts:

b	refers to base of cone
I	refers to interior ring
m	membrane solution
x	about a meridional axis
z	about a normal axis

BUCKLING MODELS

A sketch of the two models studied is given in Figure 1. The models are 120° truncated cones loaded by uniform external pressure. The resultant of the pressure load is reacted by a vertical line support through the centroid of the nose ring to simulate the inertial reaction of a payload. The effect of a nose cap is neglected.

Configuration (A) is an aluminum sandwich shell composed of three isotropic layers and no interior rings. The properties of the sandwich face layers are: $E = 10.5 \times 10^6$ psi, $\mu = 0.32$, $t = 0.020$ in. The sandwich core layer is 0.500 in. thick and is assumed to provide negligible rigidity in tangential directions while providing sufficient transverse shear and normal rigidity in order that the thin shell hypothesis of non-deformable normals remain valid.

Configuration (B) is a magnesium ring-stiffened monocoque shell composed of a single isotropic layer with 31 equally spaced identical interior rings. The properties of this layer are: $E = 6.5 \times 10^6$ psi, $\mu = 0.35$, $t = 0.051$ in. The interior rings have the same elastic moduli as the shell wall and have the following section properties: $I_x = I_z = 0.00414$ in.^{4}, $I_{xz} = 0$, $J = 0.00828$ in.^{4}, $S = 0.0635$ in.^{2}, and $Z = 0.3745$ in.

For each configuration, five cases of large end (base) rings were considered. The rings are of magnesium ($E = 6.5 \times 10^6$ psi and $\mu = 0.35$) and have the following section properties.

Case	I_x	I_z	I_{xz}	J	S	Z
1	0.765 in.^{4}	0.765 in.^{4}	0	1.53 in.^{4}	0.98 in.^{2}	1.31 in.
2	3.13	3.13	0	6.27	1.57	2.06
3	10.60	10.60	0	21.20	2.35	3.06
4	3.13	0	0	0	1.57	2.06
5	0	3.13	0	0	1.57	2.06

For each of Cases 1 through 5, a magnesium ring with cross-sectional properties of the Case 1 base ring is assumed to support the small edge of the cone. Since a normal pressure field acting on a shell with ring-supported edges is a nonconservative loading (Ref. 5), initially only "dead" pressure loading (for which the local load vectors are invariant during buckling deflections) was considered in Cases 1 through 5. An additional case, designated as Case 6, for which both shell edges are simply supported (i.e., $\eta = v = \Delta P = M = 0$) was also studied for each configuration. In Case 6, both dead pressure loading and normal pressure loading were treated.

It is well known that, in general, the use of static stability analysis yields only an upper bound to the kinetic critical load for nonconservative loading. However, in order to gain more insight into the significance of normal pressure loading, additional calculations were made for Cases 2 and 3 with this loading.

RESULTS

Prebuckled Equilibrium State

Figures 2 and 3 show the shell stress resultants and meridional rotation of the prebuckled equilibrium state obtained from linearized shell and ring theory for Configurations (A) and (B), respectively. Cases 1 and 6 are shown; Cases 2 through 5 are nearly identical to Case 1. The corresponding functions obtained from membrane theory are:

$$
\begin{aligned}
T_{1_m} &= p\left(r_b^2 - r^2\right)/2r\cos\alpha \\
T_{2_m} &= -pr/\cos\alpha \qquad\qquad (1) \\
\chi_m &= \left[(4E_1/E_2 - 1)\, r^2 + r_b^2\right] p\tan\alpha/2E_1\,\bar{t}r\cos\alpha
\end{aligned}
$$

Comparison of Eqs. (1) with the curves of Figure 2 shows that membrane conditions are never fully realized on Configuration (A). In Figure 2b the straight line representing T_{2_m} has been inserted. The fact that the edge zones in which $T_2 > T_{2_m}$ comprise 46 percent of the total length of the shell suggests that, in this case, use of the membrane prebuckled state in the stability analysis would lead to a low estimate of the buckling load.

In Tables 1 and 2 are given the ring hoop forces of the prebuckled equilibrium state for Configurations (A) and (B), respectively. In these tables, the rings are numbered in the order encountered as the shell meridian is traversed starting at the small end. In Table 2, omitted values for Cases 2 through 6 are unchanged from the corresponding values for Case 1. Although not used in the stability analysis, the prebuckling bending moments of the end rings are shown in Tables 3 and 4 for Configurations (A) and (B), respectively. The ring torsional moment is not shown since it is identically zero for axisymmetric deformations.

In the case of Configuration (B), Eqs. (1) represent the membrane response of an equivalent orthotropic shell. Therefore, the average effect of the prebuckling ring hoop forces of Table 2 should be added to the circumferential stress resultants of Figure 3 before comparing with $T2_m$. In this case, it is seen that over most of its interior, the shell is responding effectively as an equivalent orthotropic membrane shell for which $E_2/E_1 = (td + A_I)/td = 1.69$.

The curves of Figures 2 and 3 may also be used to check qualitatively the validity of the linearized prebuckling equilibrium state used in the stability analysis, since the basic assumption underlying this approximation is that at the critical load $1/2\, \chi^2 \ll e_1 = (T_1 - \mu T_2)/Et$ in regions of significant buckling response.

Buckling Modes

Table 5 gives the calculated external critical pressures.* The values which are shown in parentheses for Cases 2 and 3 include the effect of prebuckling rotations, whereas all other values neglect this effect. Because of the smallness of this effect [at most, 4 percent for Configuration (B), Case 3] the less precise values of critical pressure shown for Cases 1, 4, 5, and 6 are considered adequate, and the extra work required to improve them unwarranted.

Since normal pressure loading is nonconservative in Cases 1 through 5, it is not known with certainty that the values obtained for this loading in Cases 2(N) and 3(N), n = 2, are true kinetic buckling pressures. However, these values, being upper bounds to the kinetic buckling pressures, represent more accurate results for n = 2 buckling than those obtained for the same cases assuming dead pressure.

*Normally, for a given value of n the computer solution converges to the buckling mode with the minimum critical pressure in absolute value. In some cases the critical pressure obtained was negative, indicating that, for the given value of n, internal pressure causes buckling at a lower value than external pressure. At the same time the calculation furnished a lower bound to the external critical pressure. In most of these cases this lower bound was higher than the actual external critical pressure occurring at a different value of n, and these lower bound values are shown in Table 5 preceded by a greater than sign (>). On the other hand, if it is necessary to obtain the external pressure buckling mode for the given value of n, it can be found by either of the techniques of eigenmode orthogonalization or eigenvalue shifting. This was required for Case 2, Configuration (B) for n = 2, for which the buckling mode was obtained by eigenvalue shifting.

Figures 4 and 5 show the incipient buckling mode displacements for Configurations (A) and (B), respectively. Cases 1, 3, and 6 are shown; Cases 2, 4, and 5 are nearly identical to Case 1. The corresponding functions for inextensional deformation are:

$$
\begin{aligned}
u &= Ar_b \\
v &= Br - nAr_b/\sin\alpha \\
w &= (n^2 - \sin^2\alpha)Ar_b/\sin\alpha\,\cos\alpha - nBr/\cos\alpha
\end{aligned}
\qquad (2)
$$

Comparison of Eqs. (2) with the curves of Figures 4 and 5 show that for Cases 1, 2, 4, and 5, the buckling mode is essentially inextensional. Since flexural strain energy is smaller than extensional strain energy roughly by a factor t^2, the natural tendency for thin shells is to buckle (or vibrate) in an inextensional mode, if it is kinematically admissible. In fact, for n = 2, there is very little difference between the buckling mode shapes of Cases 1, 2, and 3. It follows that the flexural strain energy of the base ring in its buckled state essentially controls the corresponding critical pressures. Since the (flexural) section properties of the base rings of Cases 1, 2, and 3 vary in the same proportion, the second harmonic critical pressure for these cases varies approximately in a linear fashion with the base ring flexural rigidity.

On the other hand, for sufficient base edge constraint, the governing buckling mode has seven circumferential waves, as in Cases 3 and 6. In this mode of buckling, the shell develops high extensional strain energy, whereas the edge rings develop relatively little strain energy, evidenced by the small buckling displacements at the edges. Consequently, the corresponding critical pressures are relatively insensitive to the edge conditions.

Similar results have previously been reported in Ref. 2 for cylindrical shells with ring-stiffened edges. However, the result of Ref. 2 that the critical load for cylindrical shells is essentially independent of the out-of-plane ring flexural rigidity has no counterpart for conical shells. This fact is illustrated by the results for Cases 4 and 5, which show that for Configuration (A) I_x (of the base ring) is more efficacious than I_z, whereas for Configuration (B) the reverse is true.

As indicated by the buckling displacements of the ring-stiffened shell in Figure 5, some of the interior rings are relatively lax in resisting the buckling, particularly those in the vicinity of the small end of the cone. Therefore, a significant increase in critical pressure may result from a redistribution of the ring material in accordance with the distribution of buckling deflections.

In Figure 6 are plotted the critical pressures of Cases 1, 2, and 3 as a function of base ring flexural rigidity. The intersection of the curves for $n = 2$ and $n = 7$ give the minimum base ring rigidity required to suppress inextensional buckling. As the $n = 7$ curves indicate, further stiffening of the base ring is ineffectual.

The dashed curves in Figure 6 are straight lines connecting the values obtained for Cases 2 and 3 including both the effect of normal pressure and prebuckling deformations. Since the true curve including these effects is concave downward, these straight lines are conservative approximations. From Figure 6 is is seen that these effects shift the necessary EI value from approximately 40.5×10^6 lb-in.^{2} to 47×10^6 lb-in.^{2} for Configuration (A) and from 30×10^6 lb-in.^{2} to 33.5×10^6 lb-in.^{2} for Configuration (B).

CONCLUDING REMARKS

It has been shown that an inadequate base ring can result in low values of the critical external pressure for blunt conical shells typical of proposed planetary entry bodies. The minimum base ring sizes required to suppress this unwanted inextensional buckling mode for a uniform sandwich and a uniformly ring-stiffened monocoque wall construction have been determined. Of the two wall constructions studied, the sandwich construction is superior, withstanding up to 50 percent more pressure than the ring-stiffened monocoque when, for each shell, the base ring exceeds the minimum size. However, a significant increase in critical pressure for the ring-stiffened shell may result from a redistribution of the ring material in accordance with the distribution of buckling deflections.

REFERENCES

1. Seide, P., "A Survey of Buckling Theory and Experiment for Circular Conical Shells of Constant Thickness," NASA TN D-1510, December 1962, p. 401.

2. Cohen, G. A., "Buckling of Axially Compressed Cylindrical Shells with Ring-Stiffened Edges," AIAA J. 4, October 1966, p. 1859.

3. Cohen, G. A., "Computer Analysis of Asymmetric Buckling of Ring-Stiffened Orthotropic Shells of Revolution," presented at the AIAA Fifth Aerospace Sciences Meeting, January 1967.

4. Cohen, G. A., "Computer Analysis of Asymmetrical Deformation of Orthotropic Shells of Revolution," AIAA J. 2, May 1964, p. 932.

5. Cohen, G. A., "Conservativeness of a Normal Pressure Field Acting on a Shell," AIAA J. 4, October 1966, p. 1886.

TABLE 1. PREBUCKLING RING HOOP FORCES (LB)
CONFIGURATION (A), p = 1 PSI

RING\case:	1	2	3	4	5	6
1	3808.1	3808.1	3808.4	3808.0	3808.0	---
2	-510.0	-563.7	-694.8	-532.4	-459.4	---

TABLE 2. PREBUCKLING RING HOOP FORCES (LB)
CONFIGURATION (B), p = 1 PSI

RING\case:	1		2	3	4	5	6
1	4424.3	→					---
2	-24.94	→					-108.87
3	-141.42	→					-104.39
4	-114.61	→					-100.87
5	-101.32	→					-100.74
6	-100.51	→					-101.39
7	-101.78	→					-102.05
8	-102.72	→					-102.72
9	-103.47	→					-103.45
10	-104.26	→					-104.25
11	-105.11	→					
12	-106.02	→					
13	-106.99	→					
14	-108.00	→					
15	-109.05	→					
16	-110.15	→					
17	-111.28	→					
18	-112.45	→					
19	-113.65	→					
20	-114.88	→					
21	-116.14	→					
22	-117.43	→					
23	-118.74	→					-118.75
24	-120.04		-120.03	-120.03	-120.04	-120.05	-120.06
25	-121.34		-121.32	-121.30	-121.32	-121.35	-121.31
26	-122.70		-122.71	-122.72	-122.71	-122.71	-122.55
27	-124.49		-124.65	-124.75	-124.61	-124.40	-124.12
28	-127.23		-127.68	-127.97	-127.54	-126.88	-127.04
29	-130.45		-130.91	-131.28	-130.73	-129.89	-132.17
30	-129.62		-128.33	-127.71	-128.61	-129.96	-136.34
31	-131.14		-106.19	-101.98	-108.17	-117.58	-124.39
32	-70.69		-55.95	-46.06	-60.64	-82.98	-67.08
33	-213.47		-269.29	-305.55	-252.15	-170.54	---

TABLE 3. PREBUCKLING RING BENDING MOMENTS (LB-IN.)
CONFIGURATION (A), p = 1 PSI

Case	Nose Ring In-Plane	Nose Ring Out-of-Plane	Base Ring In-Plane	Base Ring Out-of-Plane
1	0	-4407.7	0	250.06
2	0	-4407.8	0	935.93
3	0	-4408.0	0	2415.6
4	0	-4407.8	425.33	736.74
5	0	-4407.7	-472.14	272.59

TABLE 4. PREBUCKLING EDGE RING BENDING MOMENTS (LB-IN.)
CONFIGURATION (B), p = 1 PSI

Case	Nose Ring In-Plane	Nose Ring Out-of-Plane	Base Ring In-Plane	Base Ring Out-of-Plane
1	0	-7627.5	0	325.78
2	0	-7627.5	0	607.24
3	0	-7627.5	0	962.55
4	0	-7627.5	325.91	564.54
5	0	-7627.5	-625.65	361.23

Note: Positive out-of-plane bending moments correspond to tensile stress in the circumferential filaments in the aft portion of the ring. Positive in-plane bending moments correspond to tensile stress in the circumferential filaments in the inside portion of the ring.

TABLE 5. EXTERNAL CRITICAL PRESSURE (PSI)

CONFIGURATION (A)

CASE / n:	2	3	4	5	6	7	8	9
1	1.16	3.29		6.83		5.73	5.97	6.51
2	3.30(3.23)	10.2		8.66		6.04		6.70
2(N)	(3.09)							
3	>9.85(9.22)	>28.1		9.22	6.79	6.18(6.08)	6.32	6.82
3(N)	(8.64)							
4	1.75	5.80		8.56		5.57		6.18
5	0.991	3.05		7.80		5.67		6.38
6	>31.3	>36.8		8.70	6.19	5.72	5.96	6.51
6(N)				8.68		5.72		6.51
				CONFIGURATION (B)				
1	0.897	>2.45		4.82		4.15		4.73
2	2.95(2.90)	9.03						
2(N)	(2.76)							
3	9.41(8.92)				4.36	4.21(4.05)	4.40	
3(N)	(8.24)							
4	0.296	0.622		>1.70				
5	0.495	1.62		>2.02				
6	>21.3				4.485	4.25	4.35	
6(N)						4.24		

Notes: a) (N) signifies normal pressure loading.
b) Values in parentheses include the effect of prebuckling deformations.
c) Values preceded by > are lower bounds. In these cases external critical pressure not found.

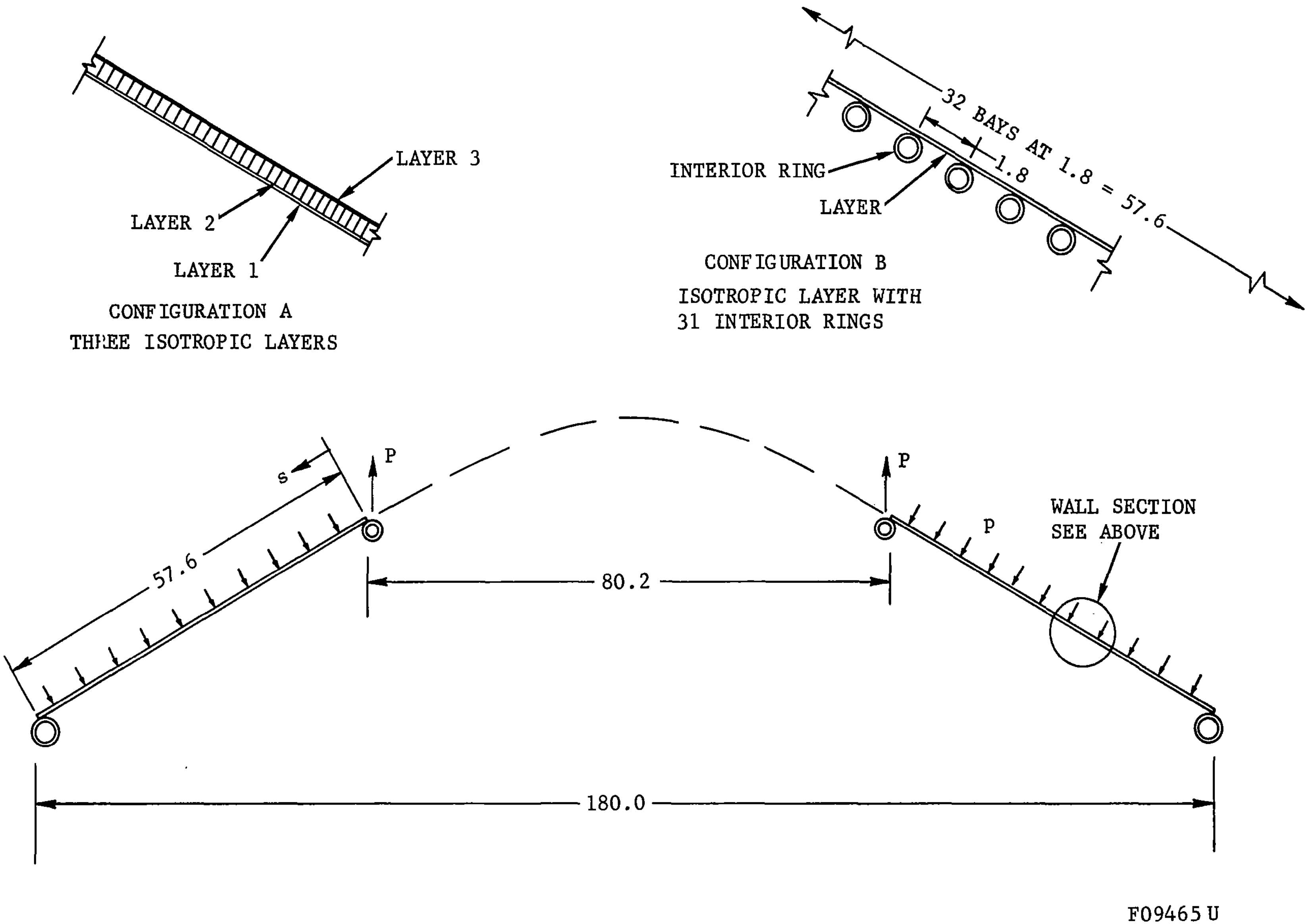

FIGURE 1. CONE BUCKLING MODELS, DIMENSIONS ARE IN INCHES

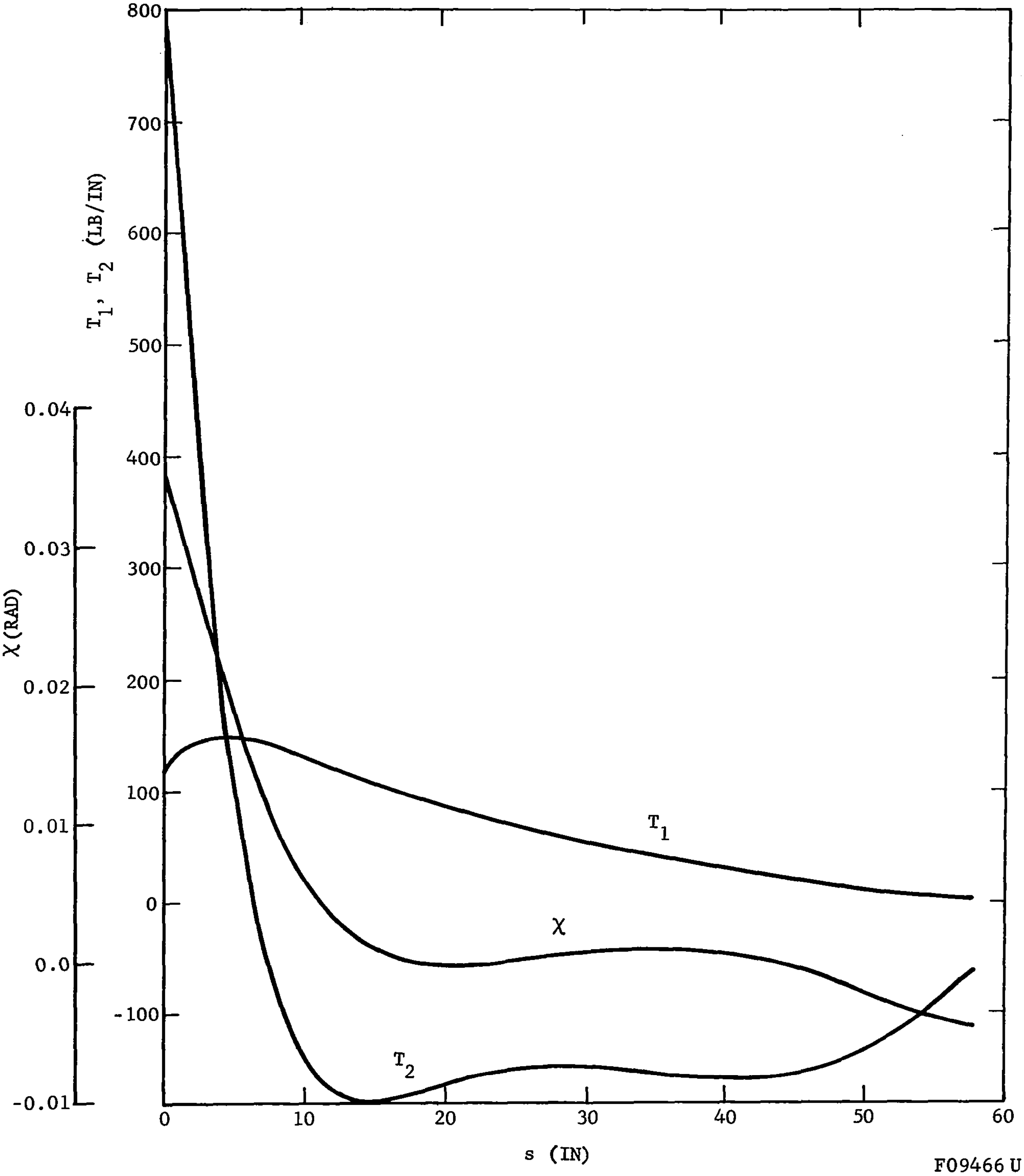

FIGURE 2a. PREBUCKLING STRESS RESULTANTS AND ROTATION CONFIGURATION A (SANDWICH CONE), CASE 1, p = 1 PSI

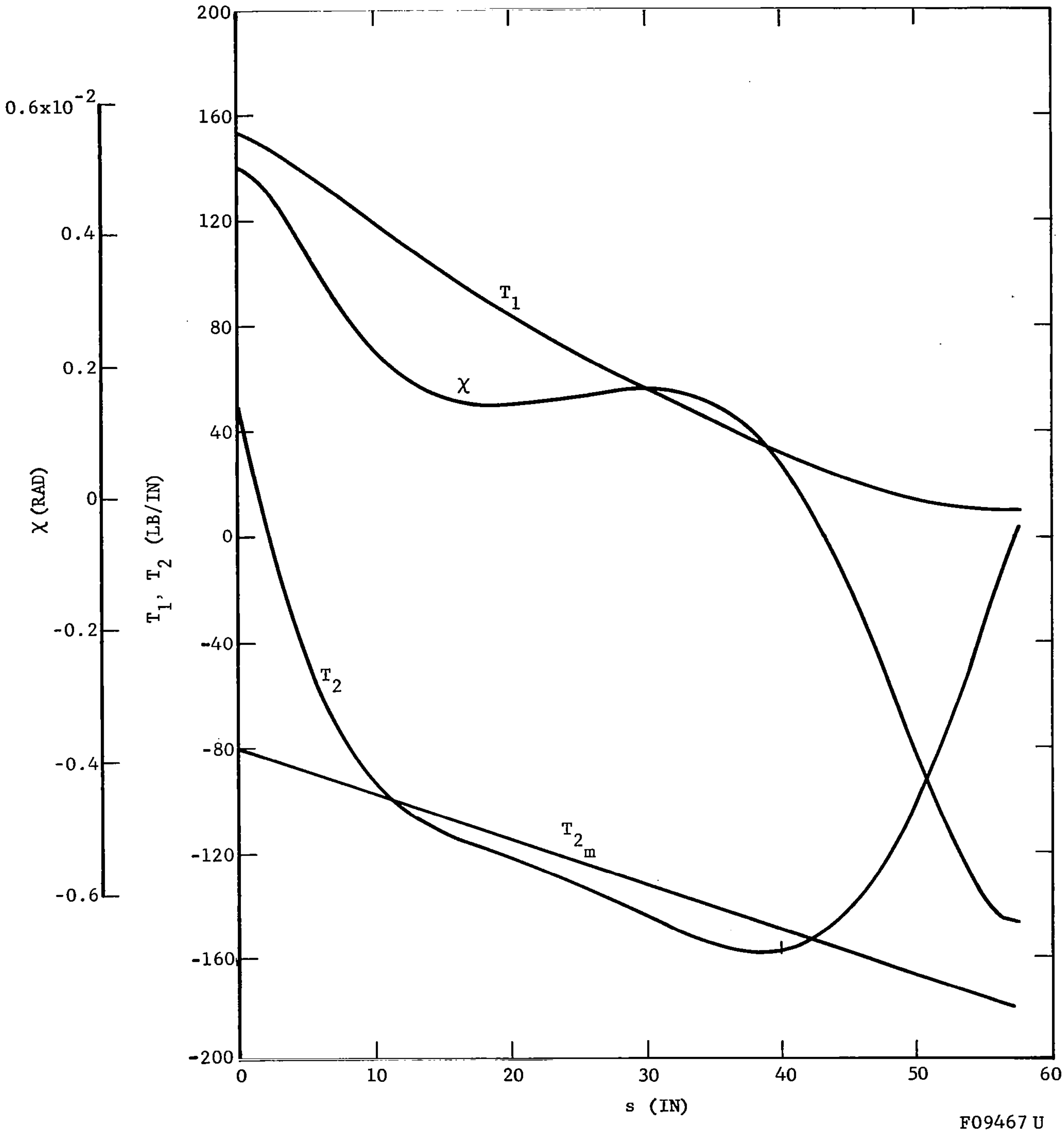

FIGURE 2b. PREBUCKLING STRESS RESULTANTS AND ROTATION CONFIGURATION A (SANDWICH CONE), CASE 6, p = 1 PSI

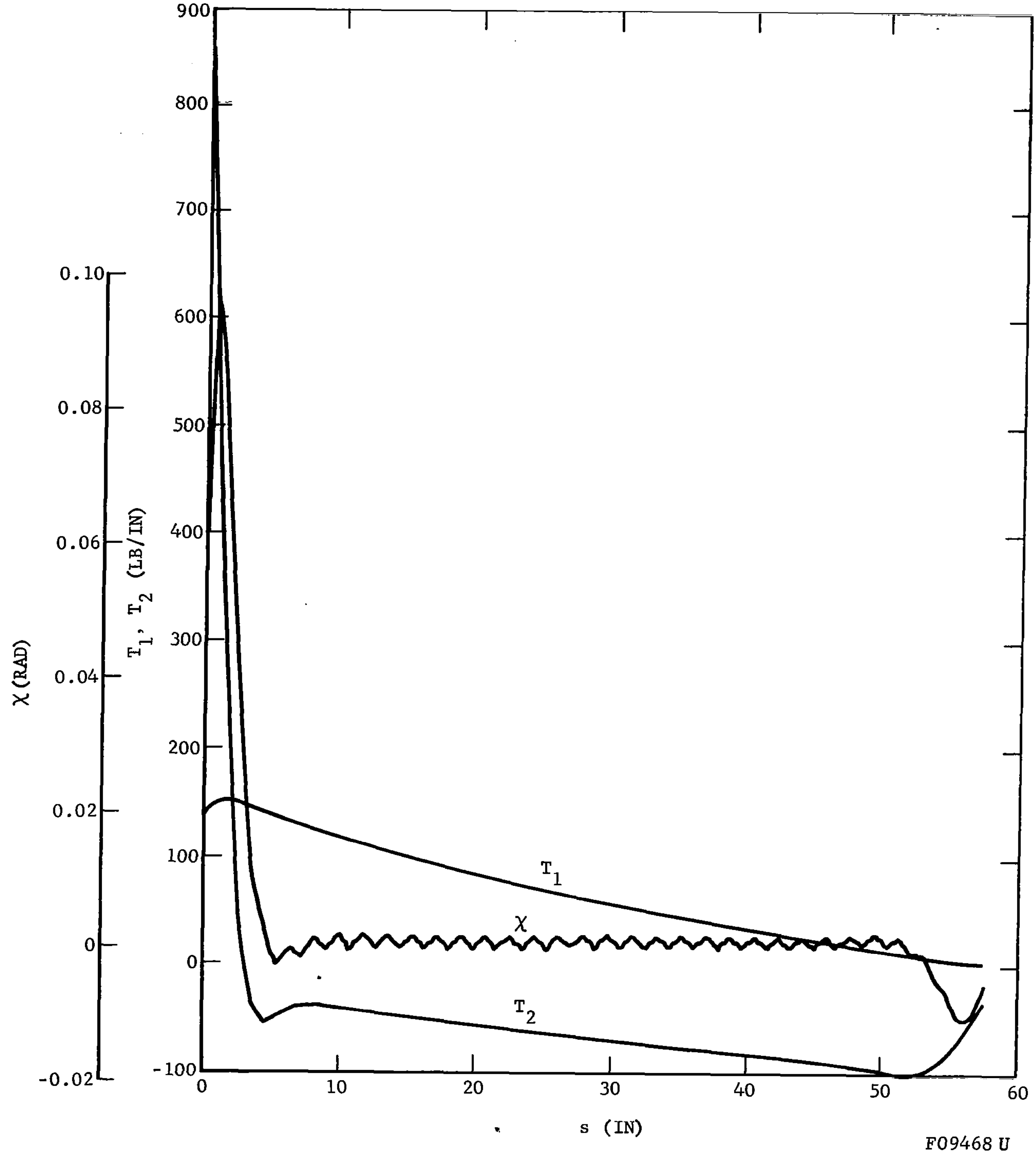

FIGURE 3a. PREBUCKLING STRESS RESULTANTS AND ROTATION CONFIGURATION B (RING-STIFFENED CONE), CASE 1, p = 1 PSI

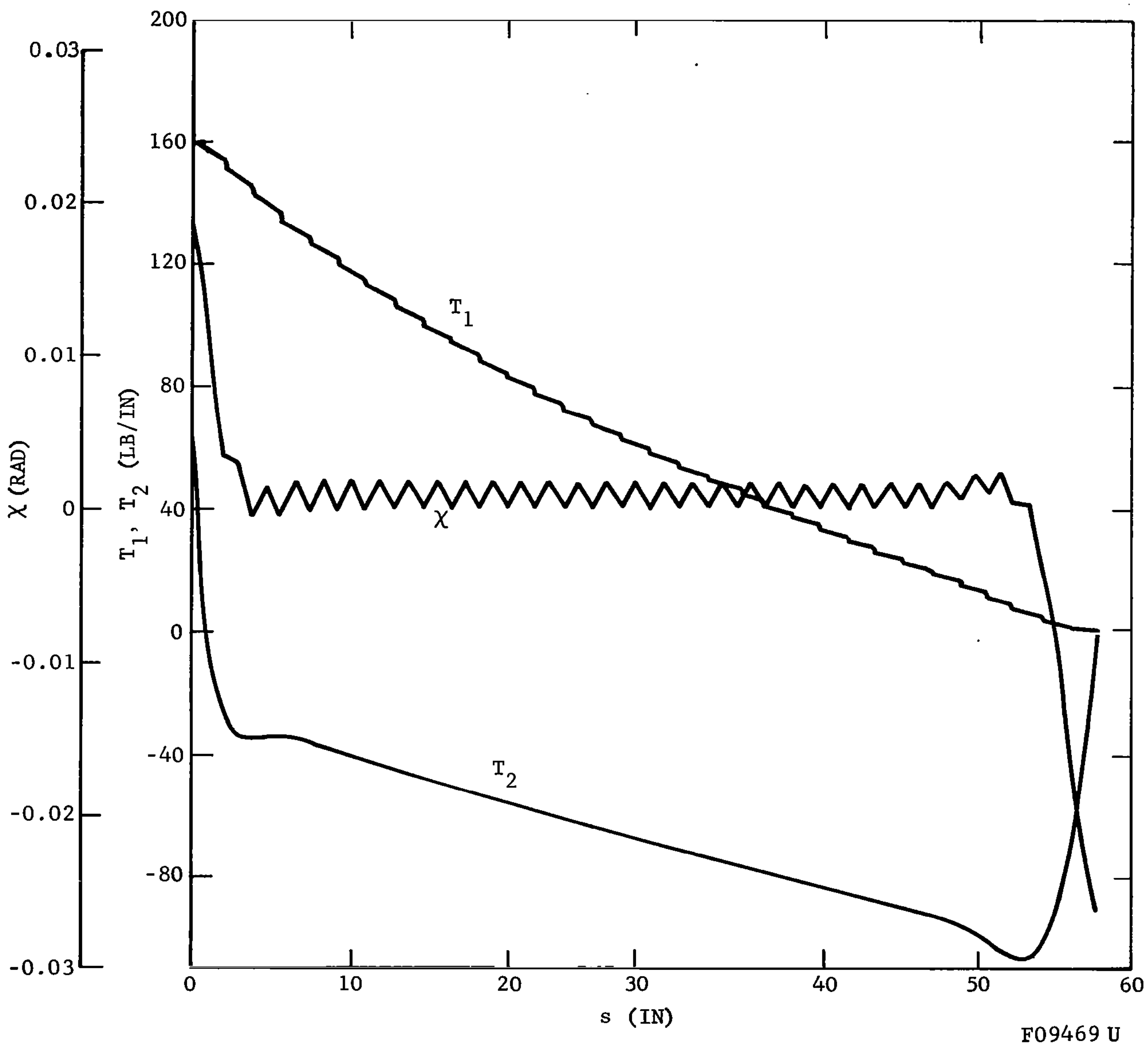

FIGURE 3b. PREBUCKLING STRESS RESULTANTS AND ROTATION CONFIGURATION B (RING-STIFFENED CONE), CASE 6, p = 1 PSI

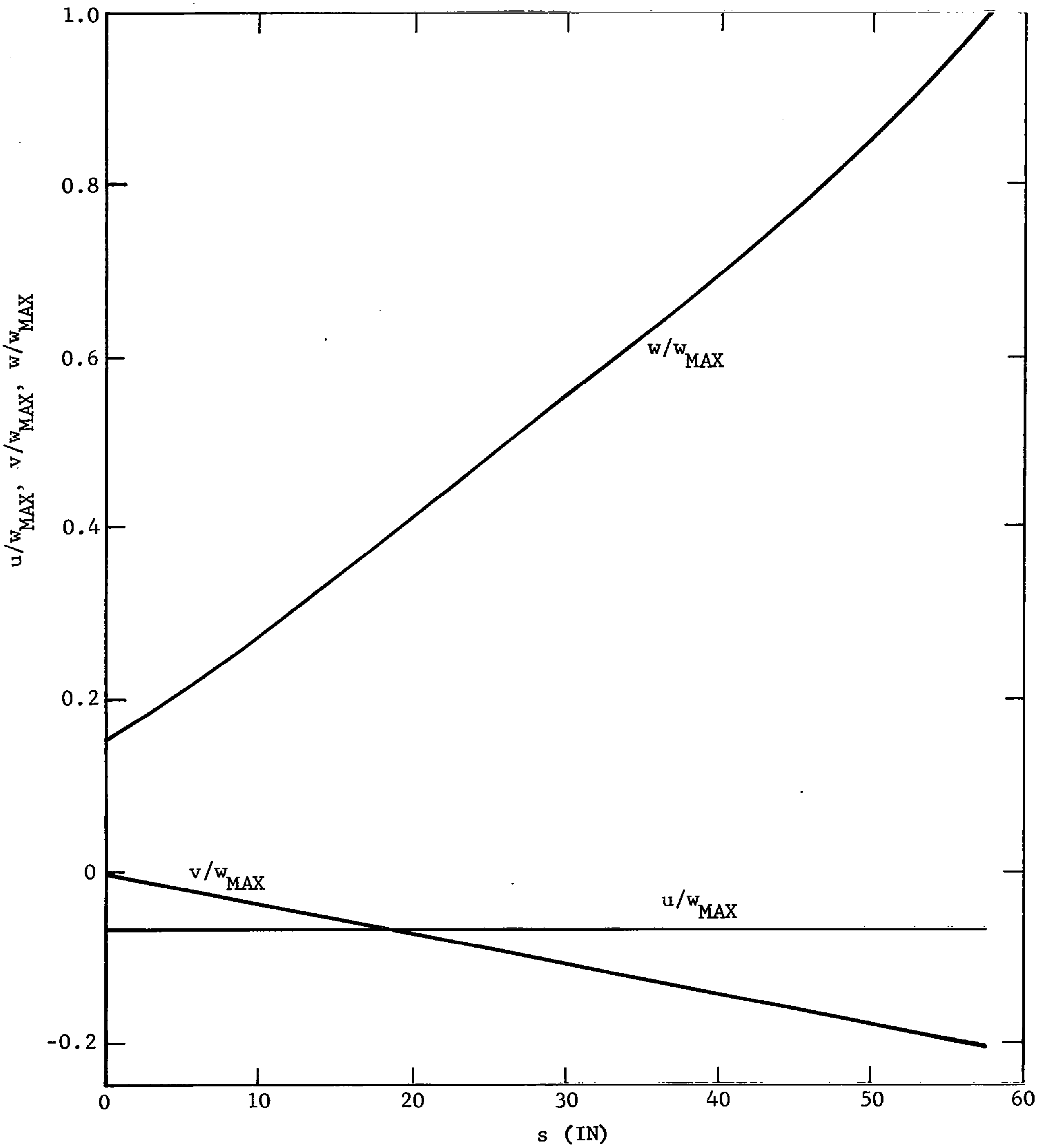

FIGURE 4a. BUCKLING MODE DISPLACEMENTS
CONFIGURATION A, CASE 1, p = 1.16 PSI (n = 2)

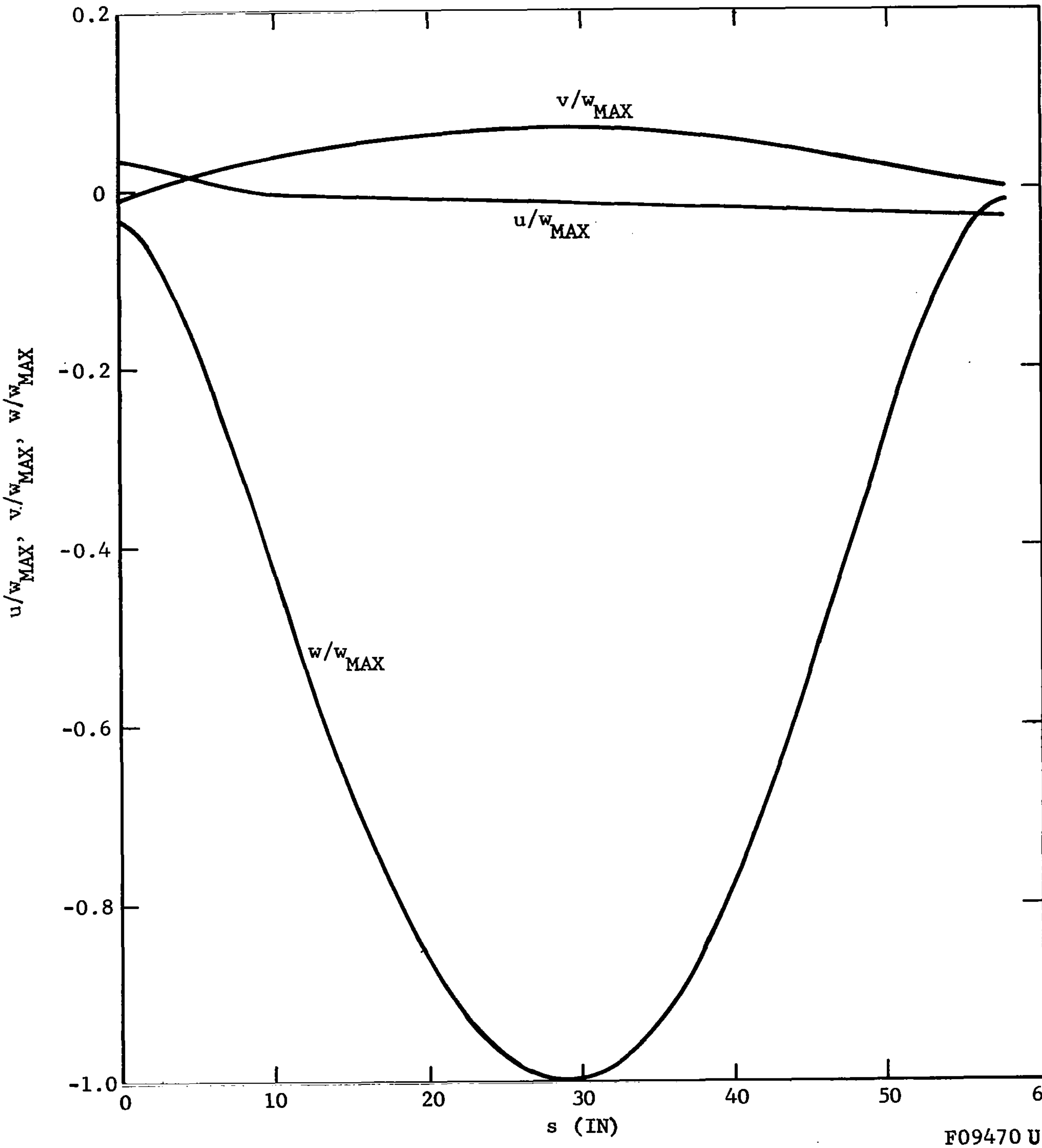

FIGURE 4b. BUCKLING MODE DISPLACEMENTS
CONFIGURATION A, CASE 3, p = 6.08 PSI (n = 7)

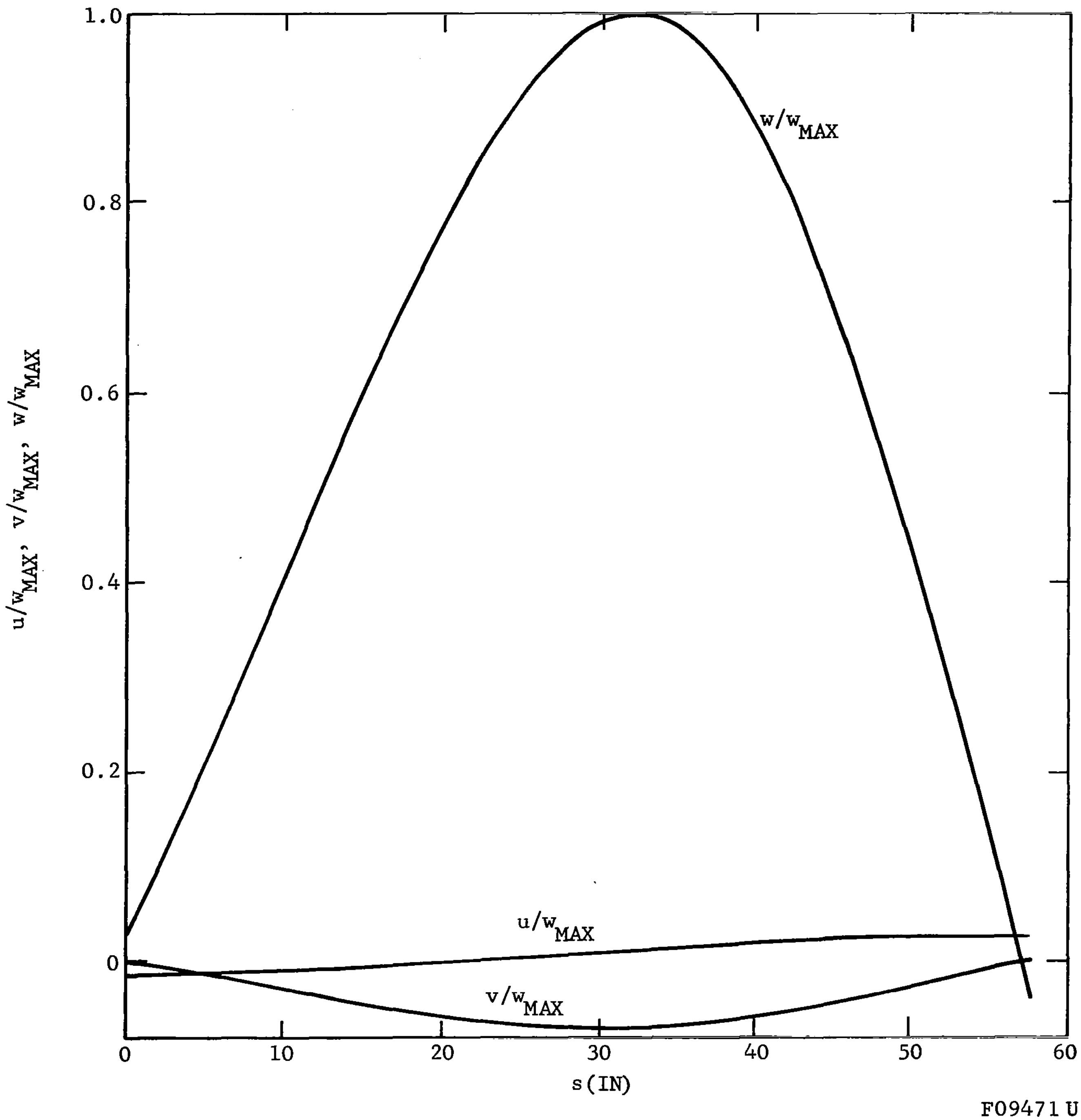

FIGURE 4c. BUCKLING MODE DISPLACEMENT
CONFIGURATION A, CASE 6 (DEAD PRESSURE), p = 5.72 PSI (n = 7)

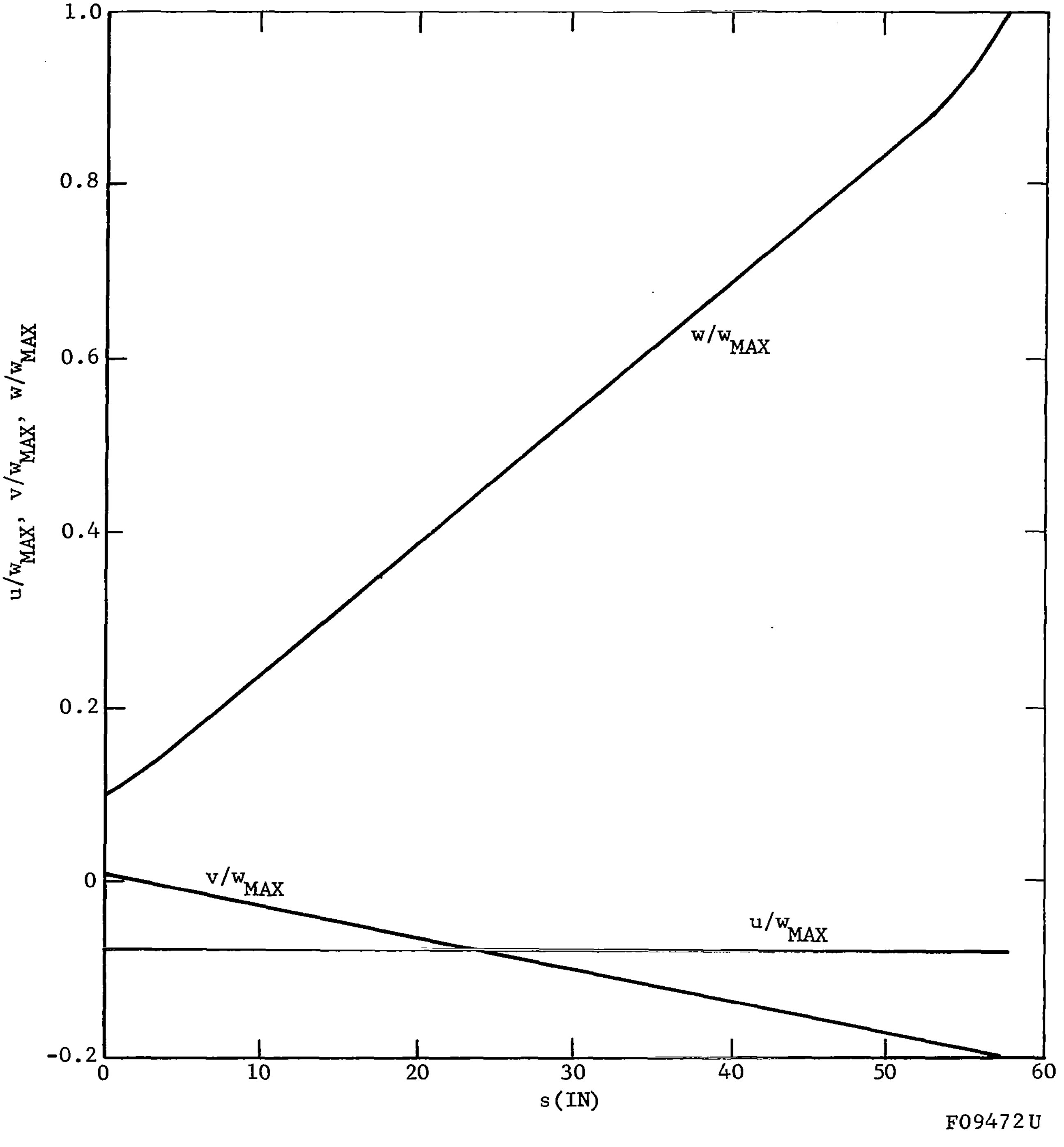

FIGURE 5a. BUCKLING MODE DISPLACEMENTS
CONFIGURATION B, CASE 1, p = 0.897 (n = 2)

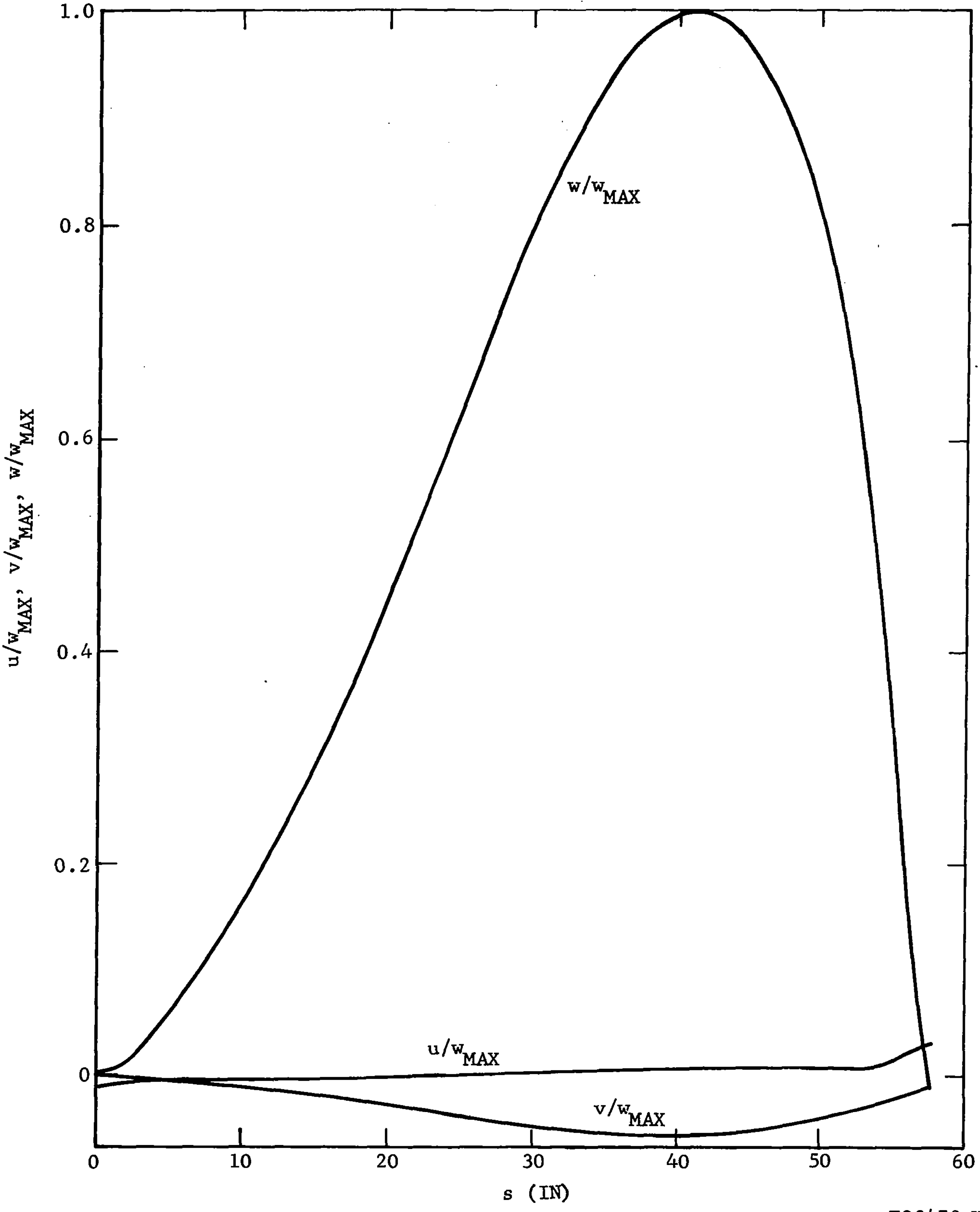

F09473 U

FIGURE 5b. BUCKLING MODE DISPLACEMENTS
CONFIGURATION B, CASE 3, $p = 4.05$ PSI ($n = 7$)

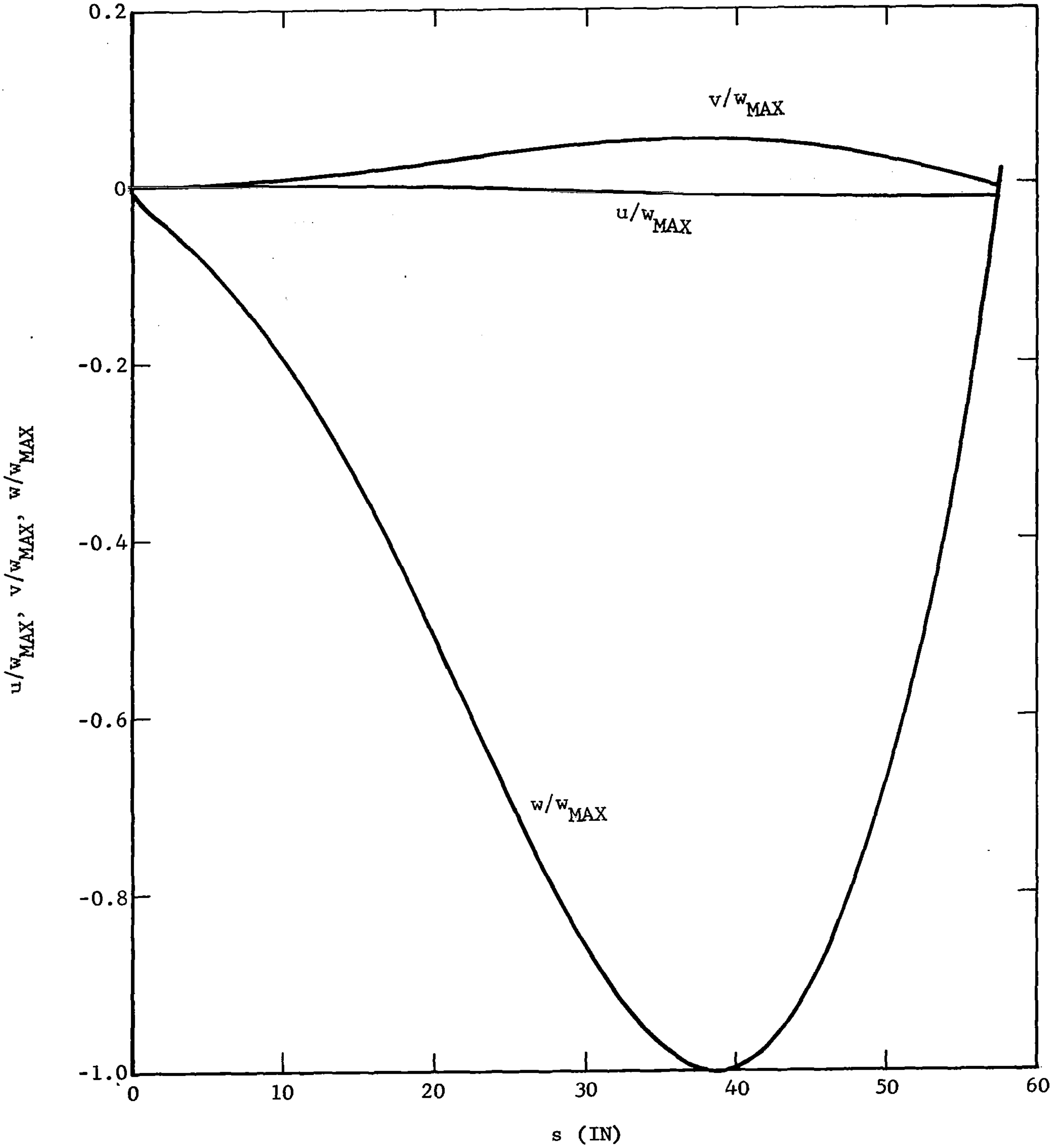

F09474 U

FIGURE 5c. BUCKLING MODE DISPLACEMENTS
CONFIGURATION B, CASE 6 (DEAD PRESSURE), p = 4.25 PSI (n = 7)

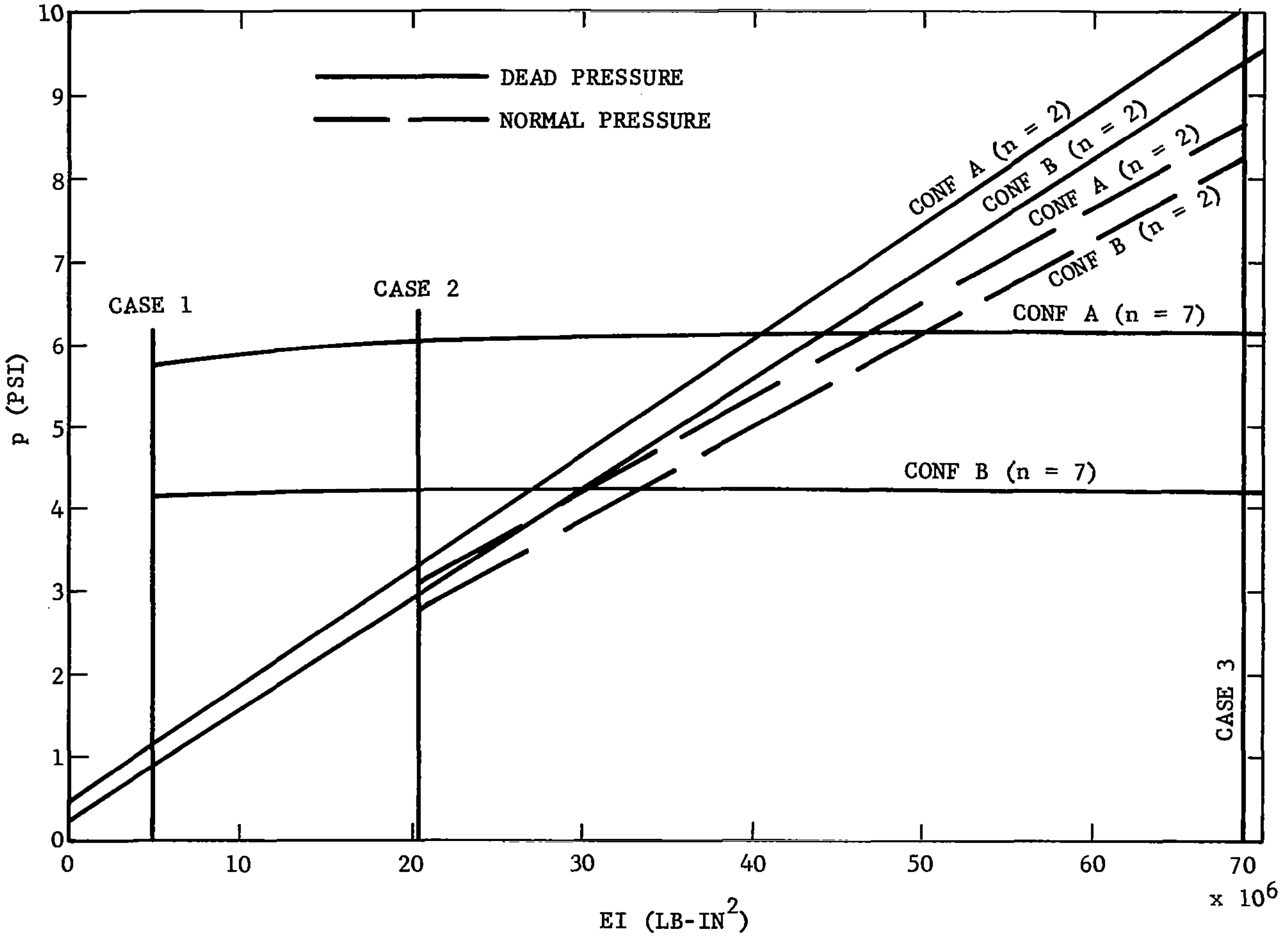

F09475 U

FIGURE 6. CRITICAL PRESSURE VERSUS BASE RING FLEXURAL RIGIDITY

NASA-Langley, 1967 —— 31 CR-795